Ultrasensitive metal-organic cluster resist for patterning of single exposure high numerical aperture extreme ultraviolet lithography applications

Manvendra Chauhan,[a] Kumar Palit,[a] Sumit Choudhary,[a] Satinder K. Sharma,[a,*] and Kenneth E. Gonsalves[b,*,†]

[a]Indian Institute of Technology Mandi, School of Computing and Electrical Engineering, Mandi, Himachal Pradesh, India

[b]Indian Institute of Technology Mandi, School of Basic Sciences, Mandi, Himachal Pradesh, India

Abstract

Background: An incredible increase in the integration of electronic chips has pushed the semicon industries to endorse high numerical aperture (h-NA ~ 0.5), extreme-ultraviolet (EUV) lithography (EUVL) ($\lambda \sim 13.5$ nm) at the commercial scale. Induction of h-NA postulates EUV resists that could outperform the resolution, line pattern roughness, and sensitivity (RLS) trade-off for chip fabricators, which is currently extremely limited.

Aim: The development of EUV resist to balance RLS trade-off as well as overcome throughput limitations of h-NA EUV system to facilitate high volume semiconductor manufacturing.

Approach: Here, we developed indium-methacrylic acid-based metal-organic clusters resist for h-NA, EUVL. To examine the h-NA single exposure patterning potential of the resist, pre-screening by sub-10 nm next-generation lithography (NGL) tools such as electron beam lithography (EBL), and helium ion beam lithography (HIBL) were conducted as a prelude to EUV exposure.

Results: Dense ~13 nm, (l/s) patterns at ~45 and ~30 $\mu C/cm^2$ were well resolved by EBL and HIBL, on the top this the line edge roughness (LER) was 2.48 ± 0.04 nm, and etch resistance ~1.98 and ~0.34 times lower than Si and SiO_2/Si systems. Also, In-MAA MOCs resist shows ultra-sensitivity of 2.3 mJ/cm^2 towards h-NA EUVL for patterning up to 26 nm half-pitch line patterns with LER ~2.36 ± 0.16 nm.

© *2022 Society of Photo-Optical Instrumentation Engineers (SPIE)* [DOI: 10.1117/1.JMM.21.4.044603]

Keywords: ultrasensitive metal-organic clusters resist; high numerical aperture; extreme ultraviolet lithography; electron beam lithography; helium ion beam lithography.

Paper 22054G received Sep. 19, 2022; accepted for publication Nov. 28, 2022; published online Dec. 27, 2022.

1 Introduction

Extreme ultraviolet lithography (EUVL, ($\lambda \sim 13.5$ nm, ~92 eV)) is anticipated to be the foremost industrial alternative for leading-edge resolutions down to N7+ logic nodes, slightly ahead of dynamic random access memory (DRAM) due to the deployment of a higher numerical aperture ~0.5 (h-NA) scanner for high volume semiconductor manufacturing (HVSM).[1] In the recent era, incessant investments have been made toward the development of h-NA anamorphic commercial-scale EUV tools, screening of ultra-sensitive thin film resists, along with alternative next-generation (NG) lab-to-fab technologies to meet the rising demand for smaller and faster high-density logic and DRAM integrated circuits (ICs) down to 10 nm or beyond nodes to pack more nano features into a single die.[2–4]

*Address all correspondence to Satinder K. Sharma, satinder@iitmandi.ac.in; Kenneth E. Gonsalves, kenneth@iitmandi.ac.in

†Current address: Charlotte, North Carolina, United States

1932-5150/2022/$28.00 © 2022 SPIE

EUVL with 0.33 NA was introduced to enable the printing of sub-16 nm, half-pitch (hp) features printing with factor $k_1 = 0.5$ for chip fabricators.[5,6] Furthermore, to enable sub-10 nm (hp) printing nodes by virtue of the same single exposure EUV, an h-NA ~ 0.5 (i.e., a 67% increase in NA), and factor $k_1 < 0.35$[4,7–10] has been adopted by Semicon industries. For the density printing of advanced nodes logic and DRAM devices, one of the key repercussions of increasing NA is that the aerial image contrast at the wafer will be higher and will aid in the printing of dense features. Also, reducing the influence of photon shot noise on image variability and pattern defects.[4] Especially, the dense contact hole arrays cannot be resolved using the 0.33 NA, EUV at resolutions below ~16 nm; therefore, double patterning is required, whereas single patterning of 0.5 NA is capable of featuring N7+ or beyond nodes.[4,11] As well, there are reports on the reduction in defects with slower resist, albeit resulting in decreased EUV exposure tool throughput, which is a critical parameter for the cost-effectiveness and feasibility of EUV benchmark productivity.

Indeed, for the maturing of EUVL for HVSM, the requisite is collapse-free high aspect ratio dense features, reasonably 2:1 ratio, high etch durability and selectivity on thinner resists, feasible with the advent of h-NA, EUV tool.[12–15] It is imperative to further extend this evolution down to 1.5-nm logic and <10-nm DRAM nodes. It is predicted that an effective decrease of depth-of-focus (DOF) with a factor of 2 to 3 with respect to the current 0.33NA,[16] engenders the need for novel ultrasensitive resists, which capture EUV photons more efficiently, and can cope with more exigent requirements of lower DOF with h-NA, optimal resolution, line pattern roughness, and sensitivity (RLS) trade-off, etch durability, and selectivity of thinner films for high-resolution (HR) dense patterns transfer of <10-nm nodes.

The biggest challenges for the successful implementation of EUVL for leading-edge logic devices and likely for futuristic fab-out DRAM, is the unavailability of compatible defect-free photoresists and mechanistic rapport to the scaling of feature size down to single-digit resolution[12,17–19] Note that there is no program to make through the direct write (maskless) tools, including electron beam lithography (EBL)[20–26] and helium ion beam lithography (HIBL) for mass production of IC chips to date.[20,27–29] It suggests maskless tools can be used to counter the scarcity of rarely accessible EUV tools to resist developers for screening/prototyping of the futuristic logic nodes resists and low-volume production. The newest, photoresists that enable sub-10 nm, hp resolution to satisfy the stringent requirements of performance and throughput imposed by the aggressive logic device-scaling are limited, even though the EUV ecosystem is ready for HVSM to the chipmakers.[30–34] In continuation with this, a photoresist must produce patterns with a line width roughness (LWR) of <20%,[35–37] which necessitates a higher dose to retain chemical noise and shot noise at a tolerable level originating from the molecular nature of resists formulation and probabilistic interaction behavior of available fewer EUV photons leading to the low-energy secondary electrons (LESEs) generation in the resists dense pattern formation.[38] In unison, the dose should be low enough ($\leq$20 mJ cm^{-2})[39] to enable high throughput chip manufacturing. However, polymer-based chemically amplified resists (CARs) have been the conventional platform and involved complex processing. The accomplishment of an expensive EUVL tool inevitably depends on the resists ability to instill the required dense N7+ logic or beyond node patterns. Today, the industry is in search of a novel resist that meets the RLS trade-off for the h-NA ~ 0.5, EUV tools.[17,30–33,40] Furthermore, the size of polymers, thin layer imaging, etch durability, etc., are considered crucial metrics to the sub-10 nm nodes. Additionally, improving the resist material's EUV light absorption is the foremost design requirement for h-NA, EUV resists platforms.[12,19,39,41] The hybrid resist offers an elegant solution to this conundrum, where the atomic level, specific entities incorporated into the resist matrix with higher EUV photon absorption cross-sections, can improve energy absorption, harvesting, mechanical strength, etch resistance, and pattern transfer by the resist, and thus, the throughput, also being formed of small formulation units that meet future resolution goals.[42–45]

To this end, several inorganic-containing hybrids resist strategies are being actively investigated for EUVL applications, largely unpopular due to the higher dose, necessary to generate solubility contrast of HR resist patterns. Metal-organic clusters (MOCs) are hybrid resist materials[20,22,42,43,46] with significant potential for NA ~ 0.5, EUVL resist platforms. Due to its considerably small molecular nature, they can attain the desired parameters for EUV photon

absorption, ultra-sensitivity, high etch resistance, and RLS trade-off while offering intrinsically small and homogenous monodisperse, size distribution by selecting the appropriate metal entities of higher EUV absorption coefficient and weaker binding ligands. In pursuance of this, our group has been extensively involved in the design and development of high-performance EUV resists development.[20,22,46]

In this work, we have developed an ultrasensitive negative tone indium-methacrylic acid (In-MAA)-based MOCs resist amenable toward h-NA ~ 0.5, EUVL applications, comprising of an indium metal core surrounded with the weakly bonded organic moiety MAA, to offer an effective solubility switching due to the cross-linking of these double bonds at the EUV photon exposure or charged particles/ions irradiations at a lower dose. A key novelty in resist is the inherent controllability of various resist parameters and ultra-sensitivity of ~2.3 mJ/cm^2 towards h-NA EUV exposure (which has been ascertained at the microfield exposure tool (MET) tool at Lawrence Berkeley National Laboratory (LBNL), United States), high contrast (γ), etch resistance and pattern transfer. EBL and HIBL exposed well-developed ~13 nm, and hp dense patterns showed the sensitivity of ~45 and ~30 $\mu C/cm^2$, respectively. Hence, the newest hybrid resist is capable of achieving high throughput of dense patterning to facilitate the production of the densest logic and memory devices for next-generation electronics development.

2 Experimental Section

2.1 *Synthesis of In-MAA MOC Resist*

Indium (III) acetate, Bis(4-tert-utylphenyl)iodonium triflate, and MAA were provided by Sigma Aldrich. Ethyl acetate, triethyl amine, and ethyl lactate were procured from Tokyo Chemical Industry (TCI) chemicals. Materials used to prepare the developer solution for the exposed In-MAA resist were propane-1-ol purchased from SD Fine Chemicals Ltd., and propionic acid procured from TCI. All of the chemicals were utilized without further purification.

The facile sol-gel process, with custom protocols, was used to make In-MAA MOC resists formulations. Primarily, two separate solutions, A and B, were prepared. Indium (III) acetate was added with ethyl acetate to make a homogeneous solution A. To make solution B, MAA, trimethylamine, and ethyl acetate were mixed. Then, solution B was gently added to solution A dropwise at 70°C while stirring continuously. The reaction was carried out at 70°C for 24 hrs, after which the final product was washed with toluene and dried at 50°C in an oven for 12 hrs. After that, the ready-to-use dry powder form of In-MAA MOC resist was kept in a vacuum desiccator to prevent it from atmospheric moisture.[46] A single crystal structure of the In-MAA MOC ($InC_{14}O_8H_{18}$) generated from the non-destructive single-crystal x-ray diffraction analysis is shown in Fig. 1(a).

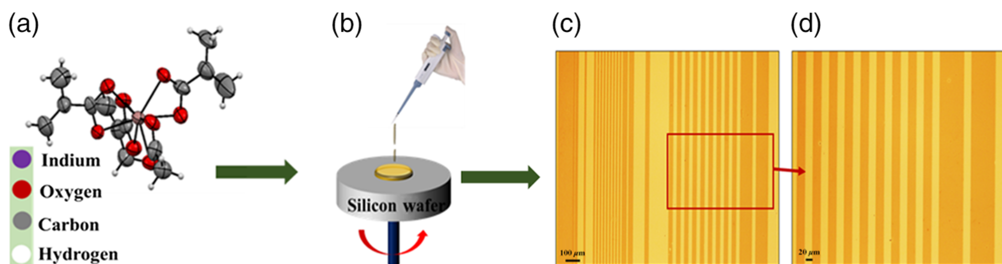

Fig. 1 (a) Single-crystal structure of designed and developed In-MAA, MOC resist formulation. Color code: gray sphere, *C*; red sphere, *O*; the purple sphere in the middle, In; white sphere, *H*. (b) Larger area uniform resist thin film formation through the cost-effective spin coating process for developed In-MAA, MOC resist formulation and (c) optical images of DUV exposed In-MAA MOC resist at 20 mJ/cm^2 at the magnification of 5× and (d) 20× for 30-μm line patterns.

2.2 *Thin Film Deposition*

With the use of a vortex mixture, 3 wt% of the newly synthesized resists and 1 wt% bis(4-tert-utylphenyl)iodonium triflate were dissolved in ethyl lactate solution. Here, the incorporation of bis(4-tert-utylphenyl)iodonium triflate in the resist solution increases the solubility of the unexposed resist in the developer solution. Also, a 3.3 wt.% excess MAA was added to the final resist solution to avoid agglomeration of the clusters and improve the self-life. The solution was then filtered using a syringe filter with a 0.22-μm pore membrane to eliminate undesirable micron-sized particles. Thereafter, the solution was spin-coated for 45 s at 3000 rpm on the set of Radio Corporation of America (RCA) cleaned silicon wafers as shown in Fig. 1(b). The coated resist films were prebaked for 45 s at 90°C to evaporate the remaining solvent. The large area of the uniform thin film thickness was found to be ~22 nm, as quantified by the thickness monitor.

2.3 *Deep Ultraviolet Lithography Exposure*

Using a standard proximity-based lithography stepper with a source power of 100 to 200 $\mathrm{mJ/cm^2}$, the In-MAA MOC resist thin film samples were exposed to deep ultraviolet (DUV), $\lambda \sim 248$-nm irradiation. After that, the DUV-exposed thin film samples were post-exposure baked at 90°C for 45 s before being developed in an optimized developer solution of 0.13% v/v propionic acid dissolved into propane-1-ol for 1 min 35 s, followed by 30 s of isopropyl alcohol (IPA) rinsing.

2.4 *Electron Beam Lithography and He$^+$ Beam Lithography Exposures*

Raith e-Line PLUS, EBL tool, and Zeiss ORION NanoFab, HIBL system were used to achieve HR dense patterns. Furthermore, the resist thin films were exposed with 20 keV, e-beam and 30 keV, He^+ beam irradiations to evaluate the HR patterning ability of the developed In-MAA MOC resist, foregoing EUV exposure. The adequately small aperture size of ~10 μm was used to achieve reduced aberration and a high DOF.[47] Henceforth, the exposed patterns were treated with custom-developed protocols of the consistent postexposure baked and development process in line, as described above for DUV lithography.

2.5 *Extreme Ultraviolet Lithography Exposure*

The developed In-MAA MOC resist set of samples was exposed to EUV radiation ($\lambda = 13.5$ nm) of photon energy 92 eV through the ~0.5 NA optics of a MET at the advanced light source in LBNL using MET standard Mask IMO410298 to evaluate the sensitivity and HR dense patterning ability of the newly designed and developed resist for high photo speed EUV applications. The resist films of ~22-nm thicknesses were utilized for EUV exposure investigations.

2.6 *Postexposure Analysis*

The surface morphology of the high aspect ratio, HR dense patterns were studied using field emission scanning electron microscope (FESEM) from Zeiss, Gemini 500 model under a 20-μm aperture at a 2.5 working distance. The reactive ion etching (RIE) system was utilized to perform the etching resistance analysis on In-MAA MOC resist thin films, and an atomic force microscope (AFM), Bruker Icon, was used to examine the film thickness as well as HR dense line-patterns topography morphology analysis. The industry-standard metrology SUMMIT software was used to measure the line edge roughness (LER) and LWR parameters for exposed dense line patterns.

3 Results and Discussion

3.1 *DUV Exposure for Resist Tone Optimization*

The In-MAA, MOC resist thin films were initially subjected to the DUV ($\lambda = 248$ nm) exposure to examine the resist film's patterning competence, ascertain the negative or positive tone nature

of the developed formulation, and subsequently, optimize an appropriate developer solution that can resolve the patterns without any residue. The freshly spin-coated (rpm: 3000; time: 45 s) In-MAA, MOC resist films over silicon <100> substrates were exposed through a hard mask at an exposure dose of $\sim 20\ \mathrm{mJ/cm^2}$ under DUV irradiation. Thenceforth, the development process for the DUV exposed resist thin films were carried out, where the concentration of solution and development time were optimized. The well-resolved negative tone line patterns shown in Figs. 1(c) and 1(d) were developed in the mixture of 0.13 v/v % propionic acid and propane-1-ol for 1 min 35 s followed by 30 s IPA rinse, custom process protocols.

3.2 *High-Resolution Prototyping: Using Maskless EBL and HIBL NG Techniques*

The maskless lithography techniques such as EBL and He^+ beam lithography are capable of patterning sub-10 nm dense resolution and are considered potential resist screening tools for NG, EUV lithography. Even if, apparently distinctions in the interaction mechanism of the high energy EUV, e-beam, and He^+ beam irradiation with resist material chemistry. Be known that the (0 to 80 eV) LESEs are always generated from aforesaid irradiation to the resist interaction and play a central role to initiate the chemical transformation of the resist.[48,49] Hence, SEs are the vital entities that triggered the exposure kinetics in the resist materials, whether the resists are irradiated under EUVL, EBL, or HIBL tools. Therefore, EBL and HIBL are next-generation tools for the early-stage screening of developed In-MAA, MOC resist formulation in the context of HR densely printing of logic and DRAM nodes down to ∼10-nm nodes or below, and optimization of sensitivity, developer and etch resistance at lower nodes.

Furthermore, R. Fallica et al. compared all these next-generation lithography (NGL) tools in their work in terms of SEs yield, relative exposure dose and reported that the HIBL mechanistic is more closely in agreement with the EUVL as compared with EBL. From the dose perspective, He^+ required approximately three times more energy than EUV photons to expose the desired poly(methyl methacrylate) resist thin films, whereas e-beam required ∼3 orders higher exposure dose.[49]

Hence, after realizing the line patterns and confirming an appropriate developer solution for the newly formulated resist as discussed in Sec. 3.1, EBL and HIBL, HR patterning was performed on In-MAA, MOC resist foregoing expensive *h*-NA, EUV exposure. A set of experiments were conducted over the resist thin films to investigate an optimal EBL dose required for HR sub-20 nm dense, well-resolved line patterning, that affirmed EBL optimum dose of $\sim 45\ \mu\mathrm{C/cm^2}$ to pattern flawless sub-20 nm, l/s densely line features, whereas the higher exposure dose ($>45\ \mu\mathrm{C/cm^2}$) leads to partial exposure of the targeted HR line-patterns proximity. The partial exposure of non-targeted area attributes to the higher number of backscattered SEs interaction with the broader exposure area of the resist film, translating into higher line widths than the virtually projected mask.[47] Therefore, In-MAA resist thin films were exposed at an optimal $\sim 45\ \mu\mathrm{C/cm^2}$, EBL dose, and exhibited the well-resolved l/s line features down to ∼13 nm, as shown in Figs. 2(a)–2(c). The computed LER and LWR for sub-20 nm l/s line patterns were 2.63 ± 0.05 and 2.8 ± 0.04, respectively. Figures 2(a)–2(c) micrographs also confirm the developer solution's ability to resolve HR (l/s) line patterns over In-MAA resist and are well optimized for defect-free densely patterning.

Moreover, the SEs induced chemical or physical reactions to enhance overall sensitivity and solubility in resist for HR feature formations. Since in HIBL a much lower number of ions undergo backscattering, which does not lead to long-range proximity effects, leads to a much more controlled manner of chemical changes in the undesirable unexposed region too.[50,51] Because critical parameter so-called electron blur in the HR dense patterning is the maximum distance away from the irradiation absorption point where electrons induce solubility switching for pattern formation, depends on the electron mean free path, what is more, the path distribution profile is strongly dependent on irradiation energy on the resist thin films.[49] Hence, In-MAA resist, patterning potential was also examined by the next-generation HIBL tool. The same resist processing parameters and film thicknesses were used for both the EBL and HIBL patterning. Figures 2(d) and 2(e) showed the defect-free dense ∼13 nm (l/s) well-resolved HIBL patterns after He^+ beam irradiation over the resist thin films at an exposure dose of $\sim 30\ \mu\mathrm{C/cm^2}$. The

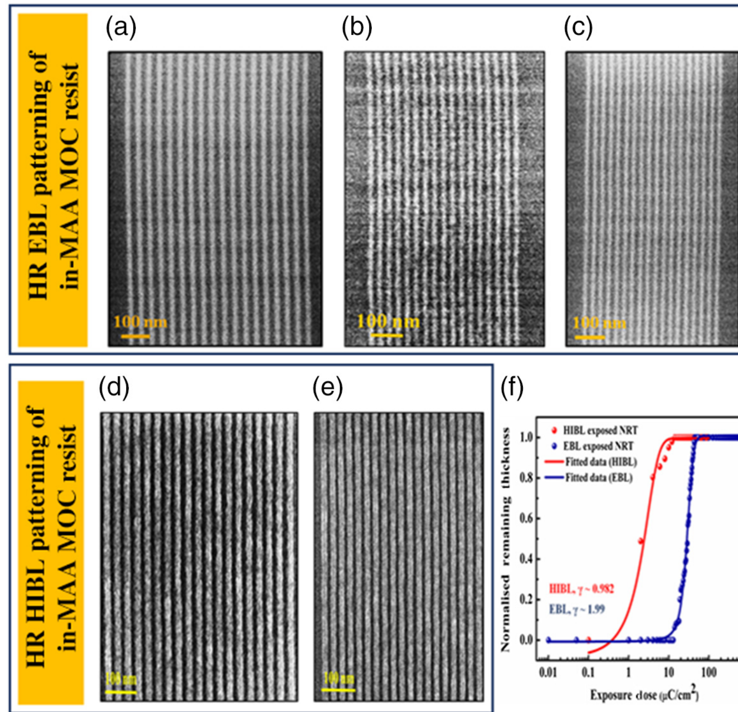

Fig. 2 EBL exposed In-MAA resist for HR dense line-patterns at 20 keV and 45 μC/cm^2: (a) 20 nm L/S, (b) 15 nm L/S, and (c) 13 nm L/S patterns. He^+-beam exposed In-MAA resist for HR dense line-patterns at 30 keV and 30 μC/cm^2: (d) 15 nm L/S and (e) 13 nm L/S patterns. (f) NRT versus exposure doses of EBL and HIBL.

computed LER and LWR for ~13 nm l/s line patterns were 2.56 ± 0.06 and 2.48 ± 0.08 nm, respectively. It attributes that in HIBL, a greater number of confined trajectory SEs or lesser blurring effects electrons were produced as compared to EBL to accelerate the chemical process in the resist thin films for HR densely features formation at a lower dose with minimal forward and backscattering.[49,52] It endorses the competency and reproducibility of the novel In-MAA, and MOC resist producing dense patterns at significantly lower exposure dose and ultra-high sensitivity. To assess further reproducibility and reliability of the MOC resist, all the processing parameters such as post-application bake and post-exposure bake temperatures, time, developer solution, and development process were kept analogous for EBL patterning as discussed in Secs. 3.1 and 3.2. After efficaciously realizing the HR EBL and HIBL patterning ability of the developed MOC resist, a set of experiments were performed to determine the remaining fraction of the resists after developing, with its specific developer solution as a function of the various EBL and HIBL exposure doses, so-called as contrast (γ) of the In-MAA resist w.r.t the EBL and HIBL exposures. A standard area of ~500 nm^2 called normalized remaining thickness (NRT) blocks were patterned over resist thin films using EBL and HIBL, respectively, where the NRT patterning exposure dose ranges for EBL and HIBL exposures were 1 to 800 μC/cm^2 and 2 to 100 μC/cm^2.

Furthermore, the computed dose-to-set (E_D) required by EBL and HIBL to expose In-MAA MOCs resists for large area patterning are ~38 μC/cm^2 and ~12.76 μC/cm^2, respectively. Also, the computed contrast (γ) for EBL and HIBL exposed large area patterns are ~1.997 and ~0.982, respectively, as presented in the experimental and fitted NRT characteristics of Fig. 2(f). The significant three-times reduction of E_D required by HIBL with respect to the E_D required by EBL to expose large area patterning on resist samples, reveals the ultra-sensitivity of He^+ interaction (HIBL) to the In-MAA, MOC resist, due to a higher number of SE_s generation and effectual contribution toward exposed resist solubility switching. There is a slight variation in MOC contrast (γ) of HIBL exposed samples in respect of EBL. Thus, it confirms the prospective candidature of in-house developed In-MAA resist for well-resolved, HR patterning with

considerably ultra-high EBL and HIBL sensitivity (<50 μC/cm^2) and is adequate to move toward EUV exposure to establish the commercial-scale readiness for densely printing of logic and DRAM, NG nodes.

3.3 *High-NA Extreme Ultraviolet Exposure and Sensitivity Evaluation*

Next-generation single exposure EUVL requires HR resist patterning for advanced nodes of dense logic and DRAM circuits with ultrahigh sensitivity and compatibility to the 0.5 h-NA, EUV tools to meet the commercial-scale, industrial standards ensuring the high throughput.[4,23] Therefore, newly formulated and EBL and HIBL pre-screened, In-MAA MOC resist coated ~22-nm thin films wafers were exposed to 0.5 h-NA EUV ($\lambda \sim 13.5$ nm, 92 eV) (MET5) lithography tool at LBNL, Berkeley, California, United States, capable of creating sufficient aerial image contrast to resolve HR dense (l/s) hp patterns.[10] Therefore, MOC resist films were prepared in analogous customized process protocols as utilized for EBL and HIBL exposures. Here, EUV exposure was performed over two sets of MOC resist samples: Sample-A (S-A), and Sample-B (S-B) of similar thicknesses but different center doses (E_0), where, E_0 for S-A was set to ~0.5 mJ/cm^2 with 0.5 h-NA, EUV exposure tool parameters: focus number: 9; flux: 3; dose number: 10; dose step and exposure type: 20 and linear. Employing this, the lowest and highest exposure dose ranges for S-A were ~0.1 and ~1 mJ/cm^2, respectively. After post-exposure standard lithographic and development processes, S-A samples were investigated under FESEM and found that the exposure dose ranges up to ~1 mJ/cm^2 is the so-called under-exposure domain for In-MAA, MOC resists.

Whereas the second set of S-B samples were exposed with EUV (MET5) tool at $E_0 \sim 10$ mJ/cm^2 of exposure parameters: focus number: 9; flux: 3; dose number: 18; dose step and exposure type: 20 and exponential. By dint of this, the lowest and highest exposure dose ranges for S-B samples were 2.3 and 51.6 mJ/cm^2, respectively. After inspection of samples under FESEM, it has been noticed that the given dose resulted in the over-exposed domain of In-MAA resist samples. Notwithstanding, the first-rate HR MOC resist patterning is shown in Figs. 3(a)–3(f) at the point-blank range of EUV dose ~2.3 mJ/cm^2.

The sensitivity response of the resist, S-A and S-B is shown in Fig. 3(g), where the relative thickness variation with respect to the EUV exposure doses of both resist samples, indicates that the EUV dose ranges from ~0.1 to ~1 mJ/cm^2 for S-A, set are ~50% of the required dose (i.e., in the range of underdose exposure). Conversely, the EUV exposure dose ranges from ~2.3 to ~51.6 mJ/cm^2 of S-B samples are saturated beyond ~2.3 mJ/cm^2 advocates the overexposure of the S-B samples.

FESEM micrographs of EUV exposed S-B samples are depicted in Figs. 3(a)–3(c). The well resolved (l/s) dense, In-MAA resist patterns resolution was limited to ~35 nm and fingerprints down to ~26 nm. Despite AFM, micrographs exhibited the HR well-resolved (l/s) resist patterning ability down to ~26 nm as divulged in Fig. 3(f). Such a dwindling in FESEM imaging might be due to the presence of a thin hydrocarbons layer over the EUV exposed samples, because the samples were imaged a delay of nearly four-plus months due to unavailability of resources. However, in tapping mode AFM imaging, the cantilever tip is excited into oscillations near the resonance frequency of the cantilever; hence the tip and sample are in intermittent contact only. The tapping mode deem to be here is more gentle and preferred for imaging of the HR In-MAA resist patterns topography analysis and did not hinder by any thin hydrocarbon layers presence and is capable of image precise surface morphological information regarding critical feature size and aspect ratio of well-resolved dense pattern arrays. As already marked, the choice of selected doses from 0.5 h-EUV photons for S-B samples engendered overexposure and impeded the HR pattering down to ~13 nm, as brought forth by EBL and HIBL. On top of the ultrahigh sensitivity ~2.3 mJ/cm^2 of the newest In-MAA, MOC resist toward EUV photons is attributed to the high atomic absorption cross-section of Indium metal ($\alpha > 10^7$ cm^2/mol) bounded with the weaker binding ligand, MAA.[44] Likewise, it might be due to a higher number of SE_s interactions with the larger surface area of the MOC resist chain. Another contributing factor may be the dramatic increase in the MOC cluster size after h-NA, EUV exposure.[53] Although, the variation in the MOC resist clusters size owing to EUV irradiation was not examined in this work. Hence,

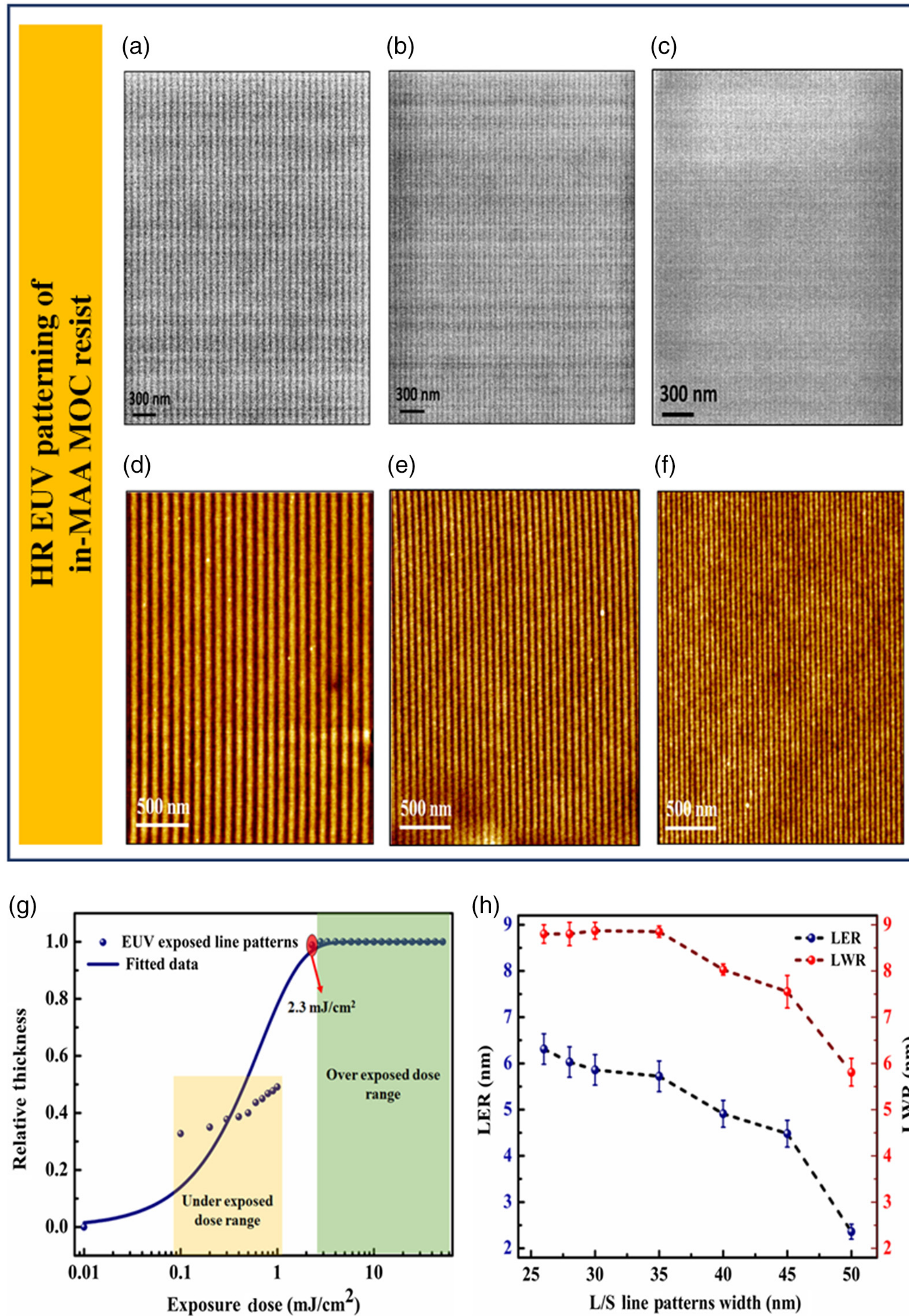

Fig. 3 FESEM images of EUV exposed In-MAA MOC resist (S-B): (a) 50 nm L/S, (b) 35 nm L/S, and (c) 26 nm L/S line patterns. AFM micrographs of EUV exposed In-MAA resist (S-B): (d) 50 nm L/S, (e) 35 nm L/S, and (f) 26 nm L/S line patterns. (g) Relative thickness versus EUV exposure doses for dense line patterns and (h) LER and LWR analysis w.r.t. the width of L/S line patterns.

it divulges that the optimal EUV exposure dose for the In-MAA, MOC resist must be amidst $\sim$2.3 to $\sim 1\ \mathrm{mJ/cm^2}$. Moreover, a relation proposed by Mark[54] supports the dependence of EUV resist sensitivity over the absorption cross-section of the resist material component. In the case of dense patterns, the analytical relation is given in the following equation:

$$E = E_o\left\{1 + \frac{1}{D_{ef}}\int_{x_o}^{x}\left(\frac{I(x)}{I(x_o)}\right)^{-\gamma}\mathrm{d}x\right\}^{\frac{1}{\gamma}}, \tag{1}$$

where E is the EUV exposure dose required to pattern line width of x by an intensity $I(x)$ on the resist exhibit contrast γ and dose-to-set (for negative tone) E_o; x_o is the center location of the line and D_{ef} is the effective thickness of resist expressed in the following equation:

$$D_{\mathrm{ef}} = \frac{1}{\alpha\gamma}(1 - e^{-\alpha\gamma D}), \tag{2}$$

where D is the actual resist thickness and α is the absorption cross-section of the resist material. The effective thickness of resist can be extracted by calculating α, γ parameters and measuring the resist thickness (D), which directly influences the EUV exposure dose as indicated in Eq. (1). Thus, a resist comprised of the entities of a higher absorption cross-section (α) will require a lower EUV exposure dose, at constant D.

Indubitably, LER/LWR is the most critical parameter of the high-resolution line patterns for advanced nodes, because the higher magnitude of LER and LWR may be lead to the logic and DRAM ICs chip failures, for instance, variability in the threshold voltage (V_{th}), higher leakage current, and variation in off-state leakage current, etc.[55,56] As per the International Roadmap for Devices and Systems (IRDS) roadmap for RLS trade-off, the LER budget is ~10% of the critical dimension.[1] In that context, the calculated LER and LWR of the l/s patterns generated over In-MAA resist after *h*-NA (0.5), EUV exposure for ~50 nm (l/s) line features are 2.36 ± 0.16 and 5.81 ± 0.3 nm, respectively, which is linearly degraded with the width of L/S line patterns as shown in Fig. 3(h). The percentage of LER for ~50-nm (L/S) dense line patterns is ~4.7%, in line with the IRDS waybill. By and large, as the line-width of HR features decreases, the LER increases, which attributes to the variation of stochastic effects caused by low absorbed photon density in the resist formulations.[37]

3.4 *Mechanistic Analysis of In-MAA MOCs Resist Formulation*

To understand the interaction mechanism of exposure irradiation-induced SEs generation within In-MAA, MOC resist, which plays a dominant role in the resist film chemical transformation, as well solubility switching due course of the development and post-exposure baking process and enables the HR pattern formation, here, the mechanistic analysis of DUV exposed MOC resist formulation was performed by x-ray photoelectron spectroscopy (XPS) for overexposed and unexposed resist thin film (~22 nm) samples to demonstrate the insights into chemical exchange, such as bond dissociation and cross-linking of the MAA ligand linked to the In metal core, accountable for the SEs generation upon DUV exposure.[57,58]

In addition, it has been anticipated that the exposure of DUV photons leads to In─C bond cleavage, which yields volatile products that outgas from the thin resist film. On that note, In─C bond cleavage may yield active In sites prone to form new bonds with neighboring activated sites and lead to the ensuing aggregation of the inorganic clusters and the creation of an insoluble network.[59–61] Figure 4 shows peaks corresponding to *C*, *O*, and In elements present in the prepared thin film and after DUV exposure. From spectra, it is evident that *O* and In intensities are elevated, whereas *C* spectra are restrained after exposure. It attributes densification of the resist layer as a result of SEs electron-induced chemical reactions in MOC resist films and engenders the formation of the HR features. These changes can be attributed to the breaking of C═C bonds of surface molecules and the formation of C─O and In-OR bonds due to cross-linking with neighboring molecules.[60] The methodology followed here, consists of the DUV exposure and is trailed by XPS analysis to provide information about the quantitative composition and elemental chemical state of the MOC resist thin films. Here, relative elemental composition (at.%) variations analyzed by the XPS spectra of as-deposited In-MAA resist for C_{1s}, O_{1s}, and In_{3d} were 57.2, 33.26, and 9.53, respectively. After DUV exposure of MOCs films, C_{1s}, O_{1s} and In_{3d} compositions were 56.16, 34, and 9.84, respectively. Hence, as postulated that during irradiation of In-MAA film, C═C bonds of In-MAA resist getting decomposed and proceeded by cross-linking with the neighboring molecules is completely supported by XPS analysis. Such chemical

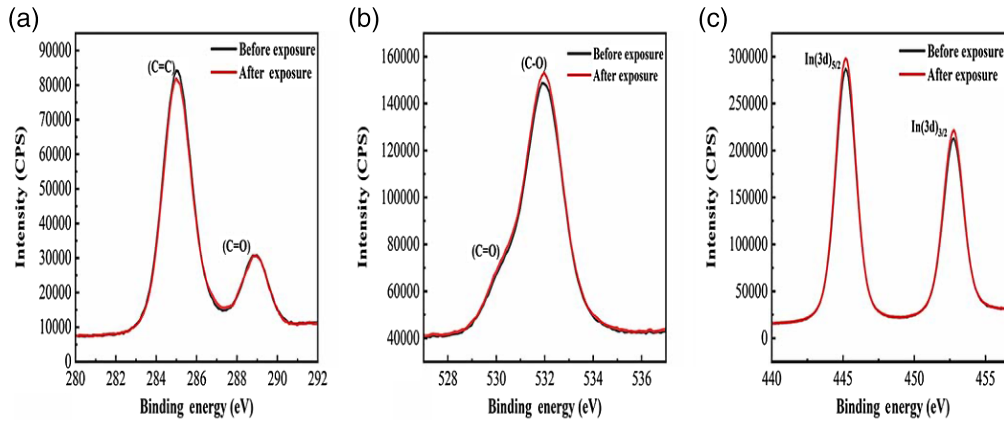

Fig. 4 HR XPS spectra of (a) *C* 1s, (b) *O* 1s and, and (c) In 3d of In-MAA MOC before and after DUV exposure.

kinetics propagation is in agreement with the cross-linking of molecular clusters ensuing hybrid molecular arrangement that becomes insoluble in the developer solution.[59,60] Furthermore, extensive EUV flood exposure photodynamic studies are planned using an appropriate synchrotron beamline with *in situ* spectroscopy.

3.5 *Ultrasensitive In-MAA, MOC Resist Etch Resistance, and Pattern Transfer for HVSM*

Although, as the electronics industry is marching toward densely ICs integration, the requirement for robust HR patterns is quintessential for next-generation technology nodes. The high etch resistance and HR pattern transfer from the newly formulated ultra-sensitive In-MAA, MOC, and EUV resist with respect to the silicon (Si) and silicon dioxide (SiO_2) are very desirable. In this context, the etch rate of the MOC resist was assessed with the Si and SiO_2/Si systems, where fluorine chemistry based on SF_6 was employed as an etching precursor of the flow rate of ~25 sccm, at ~1.5 mTorr pressure and ~60 W, radio frequency (RF) power as a reactive ion etching protocol. Using the AFM analysis, the corresponding etch rates were determined by etched depth profile on MOC resist samples as well as Si and SiO_2/Si systems. The computed etch rate of In-MAA/Si, SiO_2/Si and Si systems were 0.176, 0.35 and 0.6 nm/ sec, respectively. It indicates that In-MAA resist has a 1.98 and 0.34 times lower etch rate than Si and SiO_2/Si systems. Figure 5(a) depicts the etched depth profile of In-MAA, MOC resist w.r.t Si, and SiO_2/Si systems at various time intervals of 10, 20, 30, 40, 50, and 60 s.

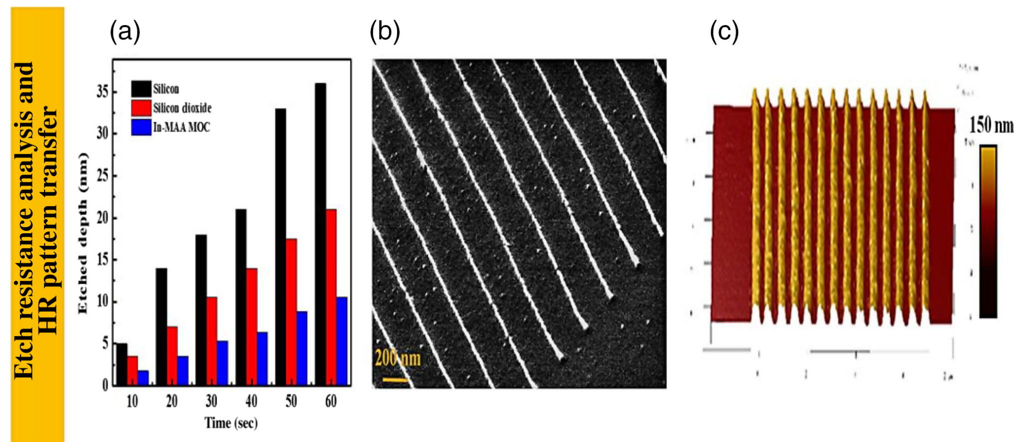

Fig. 5 (a) Etched depth versus time analysis of In-MAA MOC resists with respect to the silicon and SiO_2 substrates, (b) FESEM image of 20-nm isolated lines transferred on the silicon substrate, and (c) 3-D AFM micrograph of 20-nm isolated line patterns transferred on the silicon substrate.

With the help of HR MOC resist patterns and high etch resistance, eventually, high-aspect-ratio Si pattern transfer could be realized utilizing the customized plasma-based Si etching protocols. Hence, to transfer HR developed ~20 nm, MOC resist patterns, once more SF_6 -based fluorine chemistry was exploited and etch rate data from Fig. 5(a) were considered, where the MOC resist samples coated over silicon were exposed to SF_6 for ~120 s at the flow rate of ~25 sccm at ~1.5 mTorr. After successful resist patterns transfer on the Si, the resist residue over the etched silicon patterns was removed by ~5- min dip of the samples in ammonia solution. The topography and morphology of the HR transferred pattern over Si were examined under FESEM and AFM as shown in Figs. 5(b) and 5(c). Additionally, to more precisely visualize the thickness variation, FESEM micrographs were captured at a tilt angle of 60 deg, also contrast was adjusted such that it differentiates the transferred patterns w.r.t the bare silicon. Furthermore, the transferred patterns morphology was analyzed by AFM and depicted in three-dimensional micrograph of Fig. 5(c). It is observed that after 120 s etching, the height of the well-transferred patterns was found to be ~70 nm and confirming the MOC resist HR patterns transferability on the silicon without damaging the targeted area.

Leading, Semicon manufacturers are embarking toward utilizing the EUVL in commercial-scale production to pattern HR features in a single exposure tool, which would obviate the need for multipatterning strategies and decrease design complexity. Figure 6(a) shows the comparative analysis of the newly developed In-MAA, MOC resist, and sensitivity merits with the most promising EUV resists in practice in recent years. This analysis was based on the design principle of the resist formulations. The investigations firmly demonstrated that the sensitivity of In-MAA MOC resist formulation is the highest among in-practice EUV resists, to date. Here, it must be noted that the few of the resists compared to the present work were exposed under 0.3 NA, different mask, and illumination conditions. The role of highly sensitive EUV resists is significant for next-generation HVSM, dense logic, and DRAM devices.

Adjacent thereto, the EUVL throughput limitation associated with power losses due to the reflective optics in the optical path of the EUV photons can also be overcome by introducing ultra-high sensitive In-MAA, MOC resist for HVSM fab-line.[83] The aforementioned statement is also supported by the relation between throughput and the dose-to-set, written in the following equation:

$$T_{\text{th}} = \frac{P}{k(E_D)N}, \tag{3}$$

where k is associated with the factors related to the optical losses that occur due to the presence of reflective mirrors in the optical route of the EUV light,[83] E_D is dose-to-set for negative tone

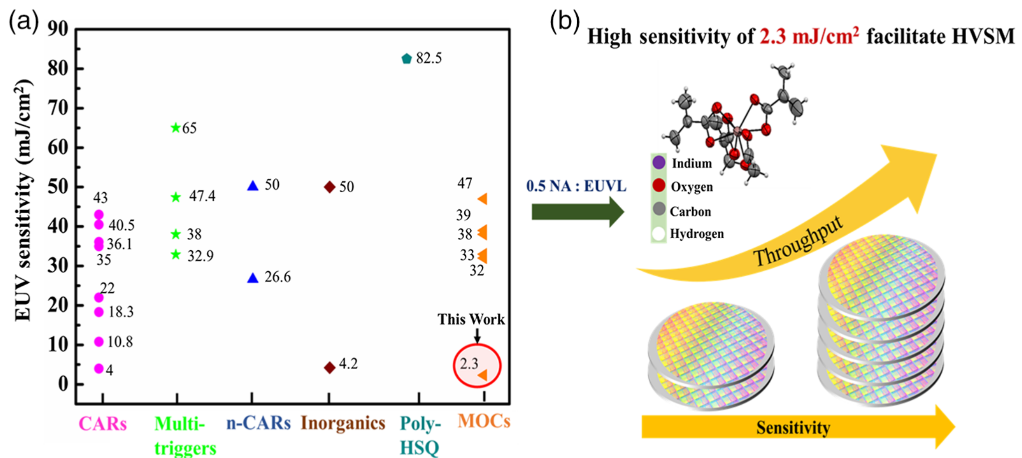

Fig. 6 (a) Comparison of various EUV resists design principles, such as CARs,[62–69] multitriggers,[70–73] n-CARs,[74,75] inorganics,[76,77] poly-HSQ,[78] and MOCs,[79–82] based on sensitivity towards EUVL and (b) pictorial representation of ultra-high EUV sensitive (2.3 mJ/cm^2) of developed In-MAA MOC resists for many folds augmentation of fab-out wafers throughput of next-generation EUVL technology.

resists, P is the power of the EUVL source, and T_{th} is the throughput of the EUVL system (wafers per hour). Here, Eq. (3) demonstrates that the throughput of the EUVL system is approximately linearly proportional to the power of the source and sensitivity of the resist material. Since the power arriving at the wafer degrades due to the absorption of the EUV light by the reflective mirrors, which lessens the intensity of the EUV light, the increment in the resist sensitivity will remain the only parameter that improves the throughput of the EUVL system. Therefore, it is safe to state that the utilization of ultra-high EUV sensitive (~2.3 mJ/cm^2) In-MAA MOC resist will surely extend the many folds of fab-out wafers, throughput as shown in the pictorial of Fig. 6(b). Undoubtedly, it would be a potential candidate and might be served as a game-changer for the next generation of EUV applications to the advanced technology nodes.

However, the prodigious ultra-sensitivity attribute shown by In-MAA MOC possibly challenges the limitations of *h*-NA EUV exposure system, leading to stochastic defects. Such feasible impediments can be diminished by tuning the sensitivity of the resist. The concept of further dilution or increasing ratios of non-Indium vinyl molecules, namely MAA w.r.t In-MAA can be utilized to modulate the sensitivity of the resist formulation. Potentially low to medium sensitivity resist formulations can be developed by varying the wt% of excess MAA added to the final solution (see Sec. 2.2), which was added to avoid potential agglomeration of the clusters. The variation in excess MAA, modulates the acidic nature of the resist solution that affects the dissolution rate of the unexposed resist area. Increasing the MAA concentration (> optimized 3 wt %) in the In-MAA MOC resist solution certainly reduces the sensitivity of the resist, but at the cost of LER/LWR degradation. The other variable is the content of photo-acid generator (PAG). Presumably, increasing the wt% of photo-acid generator (PAG) (> optimized 1 wt%) will also negatively affect the roughness of the line-patterns. Model systems assessing the reactivity ratio of these monomers, as well as PAG content, can tune the sensitivity and pattern roughness. These can be translated to EUV resist formulations for pre and actual EUV exposures.

Other ligands analogous to MAA can also be incorporated in the above-modified formulations according to their acid dissociation constant as per sensitivity requirements.[42]

4 Conclusion

In summary, an ultrasensitive, high-performance, easy-to-access In-MAA, MOC resist has been developed for *h*-NA (~0.5), EUV applications and investigated by EBL, HIBL, and EUVL performance in terms of resolution, LER/LWR, etch resistance, pattern transfer, etc. The dense line patterns of ~13 nm, L/S have been well resolved with EBL and HIBL at the exposure dose of ~45 and ~30 $\mu C/cm^2$, respectively. The computed LER values for ~13 nm patterned under EBL and HIBL were 2.63 ± 0.05 nm and 2.48 ± 0.04 nm, respectively. Furthermore, the etch resistance of In-MAA MOC resists was examined against Silicon and SiO_2/Si systems, which indicates the In-MAA resist has a 1.98 and 0.34 times lower etch rate than Si and SiO_2/Si systems. The sensitivity exhibited by In-MAA MOCs resists towards EUV photons was ~2.3 mJ/cm^2 for 26 nm highly dense line patterns. Furthermore, a fine-tuning of In-MAA MOC resists for the EUV tool to produce sub-15 nm dense lines would pave the way toward the HVSM through EUVL for semiconductor industries.

5 Appendix

Equation (3) was evaluated using the following empirical expression[83] and assumptions:

$$T_t = (T_1 + T_2 + T_3)N + T_a + T_{oh}, \tag{4}$$

where the T_t is the total time required to expose a single wafer under EUVL a system containing "N" number of fields. T_1; T_2; and T_3, respectively are the acceleration time required to attain the desired scanning speed; actual exposure time; and the time needed to reach the next field. The time required to align a wafer, i.e., T_a, and the wafer exchange time, i.e., overhead time (T_{oh}) are 5 and 6 s, respectively, which is very small and can be neglected to relate throughput with the

exposure time only. Thus, the expression 4 can be rewritten as $T_t = (T_1 + T_2 + T_3)N$; where the total processing time (T_t) can be minimized either by reducing exposure time T_2 or controlling acceleration time. The exposure time T_2 is the only variable that will be affected by the sensitivity of the resists materials exposed under EUV photon using the EUV exposure tool, whereas the other parameters are generally very small time variables that rely on the operating parameters of the exposure system. Therefore, acceleration time T_1, and stepping time T_3 can be ignored to examine the dependency of EUV exposure tool throughput to the sensitivity of the resists materials, which implies that the total time (T_t) is directly proportional to actual exposure time as $T_t \alpha (T_2)N$ or $T_t = k(T_2)N$; here, T_2, the actual time required to expose a resist material coated on the wafer is a function of E_D and P as $T_t = k(\frac{E_D}{P})N$, and T_t is related to throughput (T_{th}) as $T_{\text{th}} = \frac{1}{T_t}$.

Acknowledgment

The authors thank the Department of Science and Technology (DST) and Technology Systems Development Program (TSDP), India for financial support. Sanctioned project reference number: DST/TSG/AMT/2015/634. K.G. acknowledges access to EUV MET-5 tool at CXRO LBNL under Eureka program, and the use of the MET at LBNL is also gratefully acknowledged. The authors acknowledge the Centre for Design and Fabrication of Electronic Devices (C4DFED); Class 100 cleanroom facility, Indian Institute of Technology (IIT) Mandi, India, for various sample preparation facilities, and state-of-the-art next-generation HIBL patterning facilities for lithography work.

References

1. "International Roadmap for Devices and Systems 2021 Update Lithography" (2021).
2. P. Gargini, F. Balestra, and Y. Hayashi, "Roadmapping of nanoelectronics for the new electronics industry," *Appl. Sci.* **12**(1), 308 (2022).
3. J. van Schoot et al., "High-NA EUV lithography enabling Moore's law in the next decade," *Proc. SPIE* **1045**, 104500U (2017).
4. J. Van Schoot et al., "High-NA EUV lithography exposure tool: advantages and program progress," *Proc. SPIE* **11517**, 1151712 (2020).
5. J. Schoot et al., "High-numerical aperture extreme ultraviolet scanner for 8-nm lithography and beyond," *J. Micro/Nanolithogr. MEMS MOEMS* **16**(4), 041010 (2017).
6. P. Naulleau et al., "Status of EUV micro-exposure capabilities at the ALS using the 0.3-NA MET optic," *Proc. SPIE* **5374**, 881 (2004).
7. J. Van Schoot et al., "High-NA EUV lithography exposure tool: program progress," *Proc. SPIE* **11323**, 1132307 (2020).
8. E. van Setten et al., "High NA EUV lithography: next step in EUV imaging," *Proc. SPIE* **10957**, 1095709 (2019).
9. S.-S. Kim et al., "Progress in EUV lithography toward manufacturing," *Proc. SPIE* **10143**, 1014306 (2017).
10. C. N. Anderson et al., "Overview and status of the 0.5NA EUV microfield exposure tool at Berkeley Lab," *Proc. SPIE* **10957**, 1095708 (2019).
11. E. van Setten et al., "Imaging performance and challenges of 10 nm and 7 nm logic nodes with 0.33 NA EUV," *Proc. SPIE* **9231**, 923108 (2014).
12. X. Wang et al., "Progress in EUV resists towards high-NA EUV lithography," *Proc. SPIE* **10957**, 109570A (2019).
13. X. Wang et al., "Progress in EUV resists status towards high-NA EUV lithography," *Proc. SPIE* **11323**, 113230C (2020).
14. O. Yildirim et al., "Improvements in resist performance towards EUV HVM," *Proc. SPIE* **10143**, 101430Q (2017).
15. T. P. Allenet et al., "Progress in EUV-interference lithography resist screening towards the deployment of high-NA lithography," *Proc. SPIE* **11609**, 116090J (2021).

16. C. Zahlten et al., "High-NA EUV lithography: pushing the limits," *Proc. SPIE* **11177**, 111770B (2019).
17. C. K. Ober et al., "EUV photolithography: resist progress and challenges," *Proc. SPIE* **10583**, 1058306 (2018).
18. S. Tarutani et al., "Novel EUV resist materials design for 14 nm half pitch and below," *J. Photopolym. Sci. Technol.* **27**(5), 645–654 (2014).
19. P. P. Naulleau et al., "Critical challenges for EUV resist materials," *Proc. SPIE* **7972**, 797202 (2011).
20. R. Kumar et al., "Development of nickel-based negative tone metal oxide cluster resists for sub-10 nm electron beam and helium ion beam lithography," *ACS Appl. Mater. Interfaces* **12**(17), 19616–19624 (2020).
21. M. Yogesh et al., "Organoiodine functionality bearing resists for electron-beam and helium ion beam lithography: complex and sub-16 nm patterning," *ACS Appl. Electron. Mater.* **3**(5), 1996–2004 (2021).
22. S. Sharma et al., "All new nickel based Metal Core Organic Cluster (MCOC) resist for N7+ node patterning," *Proc. SPIE* **11326**, 1132604 (2020).
23. R. Vitor et al., "Resolution limits of electron-beam lithography toward the atomic scale accessed resolution limits of electron - beam lithography towards the atomic scale," *Nano Lett.* **13**(4), 1555–1558 (2016).
24. X. Y. Lu et al., "CO_2-based dual-tone resists for electron beam lithography," *Adv. Funct. Mater.* **31**(13), 1–9 (2021).
25. R. Glass et al., "Micro-nanostructured interfaces fabricated by the use of inorganic block copolymer micellar monolayers as negative resist for electron-beam lithography," *Adv. Funct. Mater.* **13**(7), 569–575 (2003).
26. A. Grebenko et al., "Green lithography for delicate materials," *Adv. Funct. Mater.* **31**(27), 1–10 (2021).
27. D. Winston et al., "Scanning-helium-ion-beam lithography with hydrogen silsesquioxane resist," *J. Vac. Sci. Technol. B Microelectron. Nanom. Struct.* **27**(6), 2702 (2009).
28. P. G. Reddy et al., "Heavy metal incorporated helium ion active hybrid non-chemically amplified resists: nano-patterning with low line edge roughness," *AIP Adv.* **7**(8), 085314–085319 (2017).
29. N. Ravi Kiran et al., "Resists for helium ion beam lithography: recent advances," *ACS Appl. Electron. Mater.* **2**(12), 3805–3817 (2020).
30. N. Thakur et al., "Zinc-based metal oxoclusters: towards enhanced EUV absorptivity," *Proc. SPIE* **10957**, 109570D (2019).
31. K. Kasahara et al., "EUV metal oxide hybrid photoresists: ultra-small structures for high-resolution patterning," *Proc. SPIE* **10583**, 105831P (2018).
32. H. Xu et al., "EUV photolithography: resist progress in metal–organic complex photo-resists," *J. Micro/Nanolithogr. MEMS MOEMS* **18**(1), 011007 (2018).
33. J. Haitjema et al., "Extreme ultraviolet patterning of tin-oxo cages," *Proc. SPIE* **10143**, 1014325 (2017).
34. D. De Simone, P. Vanelderen, and G. Vandenberghe, "Photo material readiness at the eve of EUVL HVM," *J. Photopolym. Sci. Technol.* **30**(5), 613–617 (2017).
35. I. Kang et al., "Line width roughness variation and printing failures caused by stochastic effect at extreme-ultraviolet exposure," *Proc. SPIE* **11609**, 116091K (2021).
36. V. Constantoudis et al., "Toward a complete description of linewidth roughness: a comparison of different methods for vertical and spatial LER and LWR analysis and CD variation," *Proc. SPIE* **5375**, 967 (2004).
37. P. De Bisschop and E. Hendrickx, "Stochastic effects in EUV lithography," *Proc. SPIE* **10583**, 105831K (2018).
38. I. Bespalov et al., "Key role of very low energy electrons in tin-based molecular resists for extreme ultraviolet nanolithography," *ACS Appl. Mater. Interfaces* **12**(8), 9881–9889 (2020).
39. T. Manouras and P. Argitis, "High sensitivity resists for EUV lithography: a review of material design strategies and performance results," *Nanomaterials* **10**(8), 1–24 (2020).
40. K. Kasahara et al., "Recent progress in nanoparticle photoresists development for EUV lithography," *Proc. SPIE* **9776**, 977604 (2016).

41. A. Moussa et al., "High NA EUV: a challenge for metrology, an opportunity for atomic force microscopy," *Proc. SPIE* **11854**, 1185410 (2021).
42. J. Passarelli et al., "High-sensitivity molecular organometallic resist for EUV (MORE)," *Proc. SPIE* **9425**, 94250T (2015).
43. D. De Simone, I. Pollentier, and G. Vandenberghe, "Metal-containing materials as turning point of EUV lithography," *J. Photopolym. Sci. Technol.* **28**(4), 507–514 (2015).
44. R. Fallica et al., "Absorption coefficient and exposure kinetics of photoresists at EUV," *Proc. SPIE* **10143**, 101430A (2017).
45. R. Fallica et al., "Absorption coefficient of metal-containing photoresists in the extreme ultraviolet," *J. Micro/Nanolithogr. MEMS MOEMS* **17**(2), 023505 (2018).
46. S. K. Sharma et al., "Development of metal-organic cluster based negative tone resist: pre-screened through the helium-ion beam prelude to extreme ultraviolet lithography (EUVL) applications," *Proc. SPIE* **11612**, 1161208 (2021).
47. R. C. Bakaraju et al., "Depth-of-focus and its association with the spherical aberration sign. A ray-tracing analysis," *J. Optom.* **3**(1), 51–59 (2010).
48. M. Rohdenburg et al., "Role of low-energy electrons in the solubility switch of Zn-based oxocluster photoresist for extreme ultraviolet lithography," *Phys. Chem. Chem. Phys.* **23**(31), 16646–16657 (2021).
49. R. Fallica et al., "Comparative study of resists and lithographic tools using the lumped parameter model," *J. Vac. Sci. Technol. B, Nanotechnol. Microelectron. Mater. Process. Meas. Phenom.* **34**(6), 06K702 (2016).
50. X. Shi et al., "Helium ion beam lithography on fullerene molecular resists for sub-10 nm patterning," *Microelectron. Eng.* **155**, 74–78 (2016).
51. D. Winston et al., "Modeling the point-spread function in helium-ion lithography," *Scanning* **34**(2), 121–128 (2012).
52. F. Luo et al., "Helium ion beam lithography (HIBL) using HafSOx as the resist," *Proc. SPIE* **9779**, 977928 (2016).
53. L. Li et al., "Studying the mechanism of hybrid nanoparticle photoresists: effect of particle size on photopatterning," *Chem. Mater.* **27**(14), 5027–5031 (2015).
54. C. Mack, *Fundamental Principles of Optical Lithography: The Science of Microfabrication*, Wiley (2007).
55. S. K. Kim, "Line-edge roughness from extreme ultraviolet lithography to fin-field-effect-transistor: computational study," *Micromachines* **12**(12), 1493 (2021).
56. R. S. Rathore and A. K. Rana, "Impact of line edge roughness on the performance of 14-nm FinFET: device-circuit co-design," *Superlattices Microstruct.* **113**, 213–227 (2018).
57. C. C. Yeh et al., "Chemical and structural investigation of zinc-oxo cluster photoresists for DUV lithography," *J. Mater. Chem. C* **5**(10), 2611–2619 (2017).
58. O. Kostko et al., "Fundamental understanding of chemical processes in extreme ultraviolet resist materials," *J. Chem. Phys.* **149**(15), 154305 (2018).
59. E. C. Mattson et al., "Chemical modification mechanisms in hybrid hafnium oxo-methacrylate nanocluster photoresists for extreme ultraviolet patterning," *Chem. Mater.* **30**(17), 6192–6206 (2018).
60. L. Wu et al., "Mechanistic insights in Zr- and Hf-based molecular hybrid EUV photoresists," *J. Micro/Nanolithogr. MEMS MOEMS* **18**(1), 013504 (2019).
61. S. Castellanos Ortega et al., "Ti, Zr, and Hf-based molecular hybrid materials as EUV photoresists," *Proc. SPIE* **10583**, 105830A (2018).
62. K. Fujiwara, "Novel EUV resist development for sub-14 nm half pitch," *J. Photopolym. Sci. Technol.* **28**(4), 519–523 (2017).
63. T. Fujii et al., "Patterning performance of chemically amplified resist in EUV lithography," *Proc. SPIE* **9776**, 97760Y (2016).
64. B. Cardineau et al., "Chain-scission polyethers for EUV lithography," *J. Photopolym. Sci. Technol.* **26**(5), 665–671 (2013).
65. H. Kudo et al., "Extreme ultraviolet (EUV)-resist material based on noria (water wheel-like macrocycle) derivatives with pendant alkoxyl and adamantyl ester groups," *J. Photopolym. Sci. Technol.* **25**(5), 587–592 (2012).

66. P. K. Kulshreshtha et al., "Harnessing entropic and enthalpic contributions to create a negative tone chemically amplified molecular resist for high-resolution lithography," *Nanotechnology* **25**(31), 315301 (2014).
67. D. P. Green et al., "Development of molecular resist derivatives for EUV lithography," *Proc. SPIE* **8679**, 867912 (2013).
68. A. Frommhold et al., "Optimization and sensitivity enhancement of high-resolution molecular resist for EUV lithography," *Proc. SPIE* **9776**, 977614 (2016).
69. A. Frommhold et al., "Novel molecular resist for EUV and electron beam lithography," *J. Photopolym. Sci. Technol.* **28**(4), 537–540 (2015).
70. G. O'Callaghan et al., "Multi-trigger resist: novel synthesis improvements for high resolution EUV lithography," *Proc. SPIE* **10960**, 109600C (2019).
71. C. Popescu et al., "Sensitivity enhancement of the high-resolution xMT multi-trigger resist for EUV lithography," *Proc. SPIE* **10143**, 101430V (2017).
72. A. P. G. Robinson et al., "High-resolution EUV lithography using a multi-trigger resist," *Proc. SPIE* **10583**, 105831L (2018).
73. C. Popescu et al., "Multi trigger resist for EUV lithography," *J. Photopolym. Sci. Technol.* **31**(2), 227–232 (2018).
74. S. K. Sharma et al., "Design and development of low activation energy based nonchemically amplified resists (n-CARs) for next generation EUV lithography," *Microelectron. Eng.* **164**(August), 115–122 (2016).
75. T. G. Oyama, A. Oshima, and S. Tagawa, "Estimation of resist sensitivity for extreme ultraviolet lithography using an electron beam," *AIP Adv.* **6**(8), 085210–085218 (2016).
76. A. Rathore et al., "Effect of molecular weight on the EUV-printability of main chain scission type polymers," *J. Mater. Chem. C* **8**(17), 5958–5966 (2020).
77. M. Trikeriotis et al., "A new inorganic EUV resist with high-etch resistance," *Proc. SPIE* **8322**, 83220U (2012).
78. T. Fujimori et al., "Novel ultra-high sensitive 'metal resist' for EUV lithography," *Proc. SPIE* **9776**, 977605 (2016).
79. M. Sortland et al., "Positive-tone EUV resists: complexes of platinum and palladium," *Proc. SPIE* **9422**, 942227 (2015).
80. Y. Zhang et al., "Dual-tone application of a tin-oxo cage photoresist under E-beam and EUV exposure," *J. Photopolym. Sci. Technol.* **31**(2), 249–255 (2018).
81. H. Xu et al., "Metal-organic framework-inspired metal-containing clusters for high-resolution patterning," *Chem. Mater.* **30**(12), 4124–4133 (2018).
82. L. Wu et al., "The role of the organic shell in hybrid molecular materials for EUV lithography," *Proc. SPIE* **10957**, 109570B (2019).
83. A. Chiba et al., "Estimation of extreme ultraviolet power and throughput for extreme ultraviolet lithography," *Jpn. J. Appl. Phys.* **40**(7), 4535–4539 (2001).

Manvendra Chauhan received his BTech degree from Invertis Institute of Engineering and Management, Bareilly, India, in 2014 and his MTech in digital electronics engineering from Madan Mohan Malaviya University of Technology, Gorakhpur, India, in 2018. Currently, he is pursuing a PhD at the School of Computing and Electrical Engineering at Indian Institute of Technology, Mandi, Himachal Pradesh, India. His research interests include advance lithography, fabrication/characterization, and reliability of materials for nonvolatile memory applications.

Kumar Palit received his BTech degree in electrical and electronics engineering from IET Bhaddal, Ropar, Punjab Technical University, Punjab, India, in 2010. From 2016 to till date, he is a technical staff in the C4DFED lab at the School of Computing and Electrical Engineering (SCEE), Indian Institute of Technology, Mandi, Himachal Pradesh, India.

Sumit Choudhary is pursuing a PhD at the School of Computing and Electrical Engineering, Indian Institute of Technology (IIT), Mandi, Himachal Pradesh, India and an MTech degree in microelectronics and VLSI design) from the Department of Electronic Science, Kurukshetra University. From 2012 to 2017, he served as an assistant professor, Kurukshetra University, India. From 2018, he joined PhD under the Visvesvaraya fellowship scheme Government of

India at IIT, Mandi, Himachal Pradesh, India. His research interests include Ge FinFET nano-fabrication comprises advance lithography and pattern transfer, nanoelectronics physics, and characterizations.

Satinder K. Sharma received his MSc degree in physics (electronic science) from HPU, Shimla, India and a PhD from the Department of Electronic Science, KUK, India. He was a visiting faculty at the Institute of Semiconductor Electronics, Stuttgart University, Germany, in 2015. Currently, he is a professor at the School of Computing and Electrical Engineering, Indian Institute of Technology, Mandi, Himachal Pradesh, India. His research interests include microelectronics circuits and system, CMOS device, nano/microfabrication, advanced lithography, sensors, and self-assembly.

Kenneth E. Gonsalves is a distinguished professor at Indian Institute of Technology, Mandi, Himachal Pradesh, India, since 2012. Prior to that, he was the Celanese Acetate distinguished professor at the UNCC from 2001 to 2014. He was also a faculty at the Center for Opto-electronics and Optical Communications at UNCC. He was an associate director of S&T Americas, Office of Naval Research Global USA, from 2009 to 2011. His recent projects on advanced nanolithography supported by US NSF, SEMATECH INT, Intel Corp., and Dow Electronic Materials.